Foam Mechanics at the Bubble Scale

D. J. Durian
Department of Physics and Astronomy, University of California, Los Angeles, California 90095-1547
(Received 19 July 1995)

By focusing on entire bubbles rather than films or vertices, a simple model is proposed for the deformation and flow of foam in which dimensionality, polydispersity, and liquid content can easily be varied. Simulation results are presented for the linear elastic properties as a function of bubble volume fraction, showing a melting transition where the static shear modulus vanishes and the relaxation time scale peaks. Results are also presented for shear stress versus strain rate, showing intermittent flow via avalanchelike topological rearrangements and Bingham-plastic behavior.

PACS numbers: 82.70.Rr, 05.40.+j, 83.70.Hq

The mechanical response of aqueous foams to applied forces is complex, exhibiting both an elastic and a viscous character. Foams behave as elastic solids for small applied shear stress and yet flow like viscous liquids at large applied shear stress [1]. Just above the yield stress, the flow is intermittent and mediated by nonlinear rearrangement events in which several neighboring gas bubbles suddenly hop from one tightly packed configuration to another. Similar geometrical packing and rearrangement phenomena dictate the mechanical behavior of such diverse systems as emulsions, colloidal suspensions, and granular media, and are reminiscent of stick-slip dynamics in earthquake faults, charge-density waves, and flux line lattices. Foams are ideal systems for studying such dynamics in that the interacting elements can be isolated and examined in the context of bulk liquid interfaces and soap films; consequently, much is known about the mechanisms for storing and dissipating energy [2]. Nevertheless, the connection between these microscopic details and the macroscopic behavior is not well understood, in part because of the importance of structure and nonlinear dynamics at an intermediate length scale set by the average bubble size.

The traditional starting point has been to consider the foam a two-dimensional periodic array of polyhedral bubbles with zero liquid content [3]. This has been generalized for computer simulation to incorporate both randomness [4,5] and a finite amount of liquid at the film junctions [6,7]. However, this approach is nontrivial to implement in three dimensions and at high liquid volume fractions; furthermore, only the static response has so far been considered. An alternative generalization incorporates both randomness [8] and realistic local dynamics [9], but focuses strictly on the motion of the film intersection points, ignoring all other degrees of freedom, and thus cannot be applied either in three dimensions or at nonzero liquid content. In this Letter, I propose a simple bubble-scale model in which randomness, dimensionality, and liquid content can all easily be varied, and demonstrate that it successfully reproduces the hallmark features of foam rheology. By explicitly introducing an intermediate length scale, this work facilitates the connection between the microscopic structure and the macroscopic behavior of an important class of materials; it also highlights the essential role played by random packing effects and rearrangement dynamics, and thus may provide insight into other systems as well.

The new model is constructed by summing pairwise interactions between neighboring gas bubbles as approximated in terms of their center positions $\{\vec{r}_i\}$ and radii $\{R_i\}$. No degrees of freedom are introduced for details of the bubble shapes, the motion of the continuous liquid phase, or the behavior of the adsorbed surfactants; time evolution of the size distribution is not allowed. The first interaction considered is strictly repulsive and originates physically in the energy cost to distort bubbles. If the distance between the centers of two otherwise isolated bubbles is greater than the sum of their radii, they will remain spherical and are assumed not to interact. If brought into contact, however, their shapes will distort and the increase in surface area will cause a repulsive central force proportional to the gas-liquid interfacial tension σ that is nearly harmonic [10–12]. This effect can be modeled by the compression of two springs acting in series where the individual spring constants scale with the Laplace pressures, σ/R_i. The second force considered is due to dissipation in the liquid between moving bubbles. It is assumed to be pairwise additive and proportional to the velocity difference of neighboring bubbles; this is the simplest form for a viscous drag. Since inertial effects are negligible, the total force on each bubble center must add to zero. The equation of motion for bubble i can then be written as

$$\vec{v}_i = \langle \vec{v}_j \rangle + \frac{F_0}{b} \sum_j \left[\frac{1}{|\vec{r}_i - \vec{r}_j|} - \frac{1}{R_i + R_j} \right] (\vec{r}_i - \vec{r}_j) + \frac{\vec{F}_i^a}{b}, \tag{1}$$

where F_0 is set by surface tension, b is set by viscous drag, and where the sum includes only neighboring bubbles j, which satisfy $|\vec{r}_i - \vec{r}_j| < R_i + R_j$. An external force, $\vec{F}_i^a$, whose components give the pressure and

 0031-9007/95/75(26)/4780(4)$06.00

shear stress, is applied to edge bubbles in order to maintain the desired volume fraction and shear strain or strain rate. The average velocity of the neighbors of bubble i is taken here as $\langle \vec{v}_j \rangle = \dot{\gamma} y_i \hat{x}$, where $\dot{\gamma}$ is the imposed shear strain rate, y_i is the coordinate of bubble i in the velocity gradient direction, and $\hat{x}$ is the unit vector in the imposed flow direction. Other choices are possible, but this is the simplest computationally, is correct in the limit of very high liquid content, and, in any case, cannot affect results for static elastic properties.

By comparison with previous models, the advantages of Eq. (1) are its simplicity and natural applicability to foams of arbitrary disorder, liquid content, dimensionality, and strain rate. And while previous models are based on a few of the fundamental rules governing the behavior of soap films and interfaces that would presumably be part of a complete *ab initio* treatment, Eq. (1) is based on a simple caricature of all such effects. Details at the soap film and surfactant scales are subsumed into phenomenological parameters, and what emerges is a microscopic relaxation time, $\tau_d = b\langle R \rangle / F_0$, set by the average bubble size and the competition between mechanisms for storing and dissipating energy. This general approach should allow reliable study of deformations and flows at length scales greater than the average bubble size. A potential drawback is that is cannot accurately describe very dry foams, since no degrees of freedom are introduced for the bubble shapes. Because the overlap of bubbles is only discouraged Eq. (1), but not forbidden, such dry-foam limiting behavior as the divergence of the osmotic pressure cannot be captured. Whereas previous attempts to incorporate finite liquid content start from the dry-foam limit, the model presented here is complementary in that it starts from the wet-foam limit.

Simulations are performed for two-dimensional square systems of $N \times N$ bubbles. As depicted in Fig. 1, the top-N and bottom-N edge bubbles are held at fixed height and relative positions, as though stuck to movable plates, while periodic boundary conditions are imposed to the left and right. The bubble radii are randomly drawn from a triangular distribution that peaks at $\langle R \rangle$ and vanishes at $(1 \pm 3/4)\langle R \rangle$; the value of $\langle R \rangle$ is chosen according to the desired liquid content. This gives a size distribution that approximates results for two-dimensional foams that coarsen by the diffusion of gas from smaller to larger bubbles. Initially relaxed configurations are obtained by first equilibrating the top and bottom edge bubbles and by next equilibrating the bulk bubbles while simultaneously translating the top and bottom edge plates. This is all done by updating bubble positions according to Eq. (1) using standard molecular dynamics simulation techniques. As evident from Fig. 1, the resulting structures closely resemble tightly packed bubbles in real foams.

To quantify the static elastic properties, two distinct experiments are performed starting from a relaxed configuration. First, a constant shear stress is applied to the edge bubbles, and the system is reequilibrated by the motion of the edge plates and bulk bubbles according to Eq. (1). Second, a small homogeneous shear step strain is imposed, and the system is reequilibrated by the motion of the bulk bubbles alone. Results for the static shear modulus G, defined as the lateral force per unit edge length, or shear stress σ_{xy}, divided by the shear strain γ, are identical for both experiments. Linearity is confirmed by changing the sign as well as the magnitude of the strain; values of G are constant throughout the range $10^{-8} < |\gamma| < 10^{-3}$. For larger strains the response becomes nonlinear, and eventually bubble rearrangements and flow are induced.

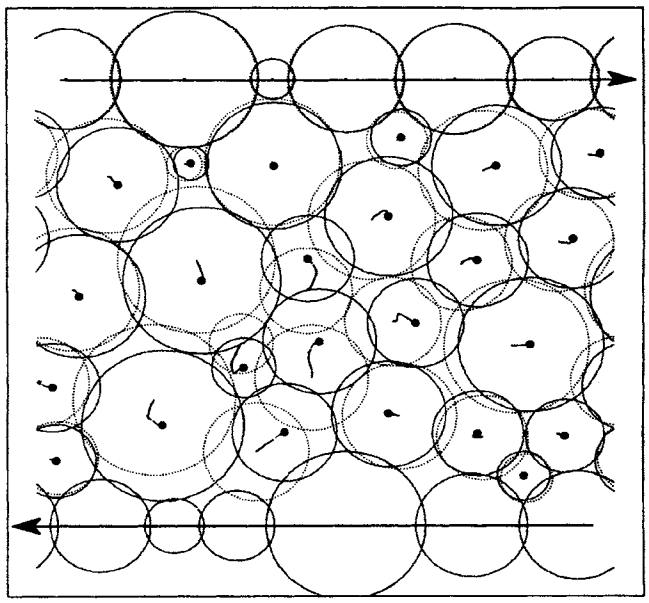

FIG. 1. Structure formed by a 6×6 polydisperse array of bubbles with $\phi = 1$. Configurations are shown before (dotted circles) and after (solid circles) a sudden structural rearrangement at constant dimensionless shear strain rate of $\dot{\gamma}\tau_d = 10^{-5}$. The bubble-center trajectories are also shown, with the final positions denoted by solid symbols.

Simulation data for G and the perpendicular force per unit edge length, or pressure P, are displayed in Figs. 2(a) and 2(b) as a function of the total area fraction ϕ occupied by gas bubbles. Evidently, both measures of the elastic character decrease for smaller ϕ and vanish continuously at a critical area fraction of $\phi_c = 0.841 \pm 0.002$. As shown by Fig. 2(c), the average number Z of spring contacts per bulk bubble decreases from about 5.5 to 3.7 as the gas fraction is lowered to ϕ_c. Such a melting, or rigidity loss, transition has been inferred from previous simulations to occur at approximately the same coordination number and liquid content [6,7,12], corresponding to random close packing of polydisperse disks. The expected critical coordination number is 4; the smaller result found here may be due to degrees of freedom lost in fixing the edge bubbles [13]. While earlier work was restricted to $\phi > \phi_c + 0.05$ and $G(\phi)/G(1) > 0.5$, the data presented here are on larger

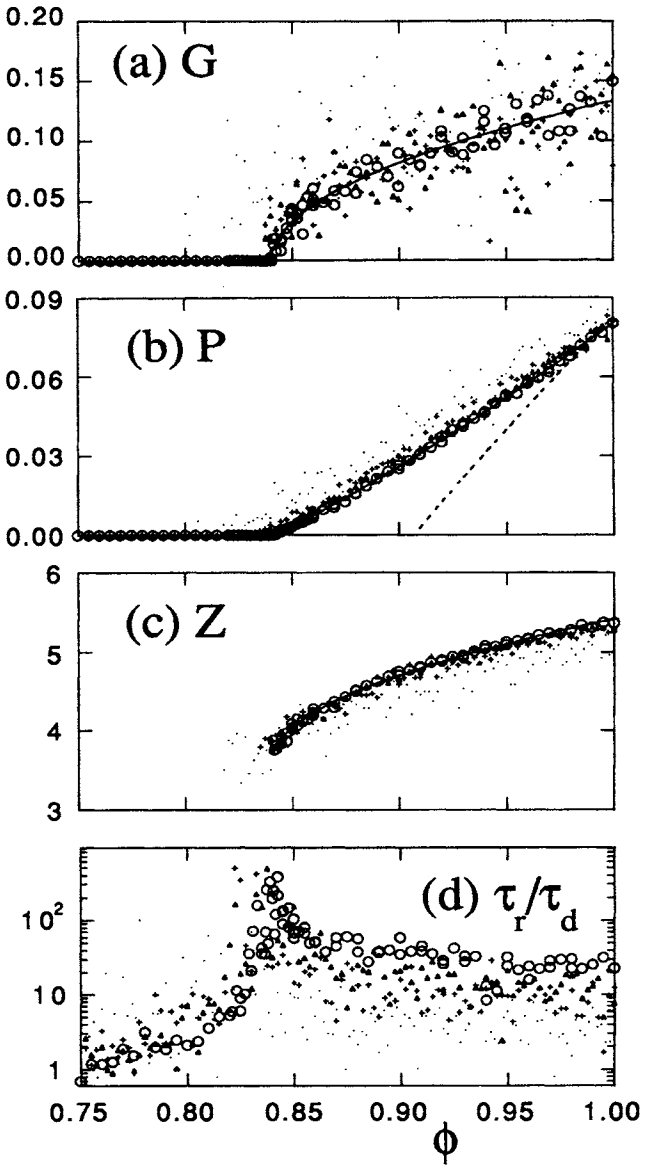

FIG. 2. Static shear modulus (a), pressure (b), coordination number (c), and stress relaxation time (d) as a function of gas area fraction. System size is $N \times N$ with N being 6 (dots), 12 (pluses), 18 (triangles), or 32 (circles). Each data point represents a different set of bubbles, and the scatter is smaller for larger systems. Solid curves represent the average behavior for the largest system.

systems and extend to both sides of ϕ_c so that the nature of the transition can be studied in greater detail.

The effect of disorder on the melting transition can be seen by comparison of the ϕ dependence in Fig. 1 with predictions for a periodic hexagonal array of uniform disks. For pressure, Eq. (1) gives $P_u = \sqrt{3}(1 - \sqrt{\phi_u/\phi})$ where $\phi_u = \pi\sqrt{12} \cong 0.9096$. As shown by the dashed curve in Fig. 2(b), this has the same magnitude and approximately linear ϕ dependences as the simulation data. While disorder has only slight influence on pressure, it more dramatically alters the magnitude of the shear modulus and how it vanishes. For uniform disks, Eq. (1) gives $G_u = \sqrt{3}(\sqrt{\phi/\phi_u} - 3/4)$, which increases discontinuously at the melting transition from $G_u(\phi_u^+) = \sqrt{3}/4$. By contrast, the shear modulus data in Fig. 2(a) are typically smaller by a factor of 4, and, to within statistical uncertainty, vanish continuously at ϕ_c.

The behavior of both P and G can be understood in terms of the average number Z of spring contacts per bubble. Above the melting transition, this coordination number varies empirically with gas content as $Z - Z_c \propto (\phi - \phi_c)^\theta$ where $\theta = 0.5 \pm 0.1$, as shown by the solid curve in Fig. 2(c). Physically, the pressure should be proportional to both the average number of springs per bubble and their average compression, $P \propto Z(\phi - \phi_c)$. This form, shown as a solid curve in Fig. 2(b), agrees well with the simulation data. For the shear modulus, the simulation data are well described by $G \propto (\phi - \phi_c)^\theta$, shown as a solid curve in Fig. 2(a). This supports the rigidity percolation picture of the melting transition, where $G \propto Z - Z_c$ is expected for two dimensions [6]. As the liquid content is increased, contacts are lost and the modulus decreases, finally vanishing when a network of compressed bubbles no longer percolates across the sample. Recent measurements on monodisperse emulsions show, by contrast, that the shear modulus and osmotic pressure have similar ϕ dependence, inconsistent with rigidity percolation [11]. The main differences between the experiments and the simulations conducted here lie in the dimensionality and polydispersity of the systems studied. Thus, it would be interesting to perform further simulations of Eq. (1), systematically varying the polydispersity in both two and three dimensions.

During the step-strain measurements of Figs. 2(a) and 2(b), data were also collected for elastic energy vs the time after the imposed deformation. This relaxation always showed a slow initial decay followed by an exponential cutoff. The time constant τ_r for the final relaxation is displayed in Fig. 2(c). For gas fractions far below ϕ_c, τ_r approaches τ_d, indicating that all relaxation is from pairs of bubbles brought into contact by the step strain, while far above ϕ_c, τ_r is larger and approaches a constant that depends on the system size. As the melting transition at ϕ_c is approached, from either above or below, the relaxation time reaches a maximum. This suggests the presence of a diverging length scale, consistent with rigidity percolation. It could also reflect the difficulty of a glassy system in finding the minimum-energy configuration. In any case, the data of Fig. 2(c) show that when the static shear modulus vanishes below ϕ_c, the foam does not simply melt into a Newtonian fluid; rather, it changes from a viscoplastic solid into a viscoelastic liquid.

Consider the dynamics of bubbles while the foam is being sheared macroscopically at a steady rate, $\dot{\gamma}$. By con-

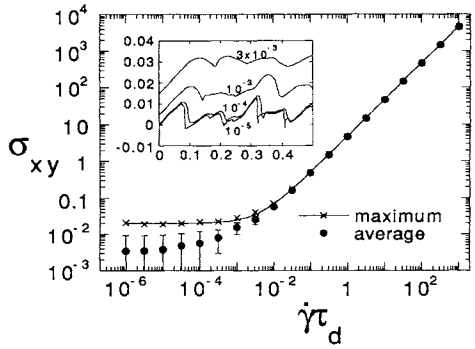

FIG. 3. Average and maximum stress vs dimensionless applied shear strain rate, taken over $0 < \gamma < 10$ for the array of bubbles shown in Fig. 1. Error bars denote rms fluctuations about the average, and the solid curves is a fit to Bingham-plastic behavior. The inset shows the actual stress vs strain for several dimensionless strain rates as labeled.

trast with the linear behavior above, steady shear flow involves large scale motion and topological rearrangements of neighboring bubbles. An example of such an event is shown in Fig. 1 for a small system at dimensionless applied shear strain rate, or Deborah number, of $\dot{\gamma}\tau_d = 10^{-5}$. Evidently the rearrangement even consists of a core of bubbles that undergo topology change surrounded by a halo of bubbles with fixed neighbors that respond elastically. Similar events have been seen in earlier simulations [7,9], and have also been detected experimentally by diffusing-wave spectroscopy [14–16]. As depicted in Fig. 1, they are avalanchelike in that the bubble motion is sudden on the time scale for noticeable plate motion.

The avalanchelike nature of rearrangements can also be seen by sudden drops in either the shear stress or the total elastic energy as a function of time. The inset of Fig. 3 shows the shear stress σ_{xy} vs shear strain, $\gamma = \dot{\gamma}\tau$, for the same system of bubbles as in Fig. 1 driven at various rates. All exhibit an initial linear increase, consistent with the previously measured static shear modulus, followed by considerable fluctuations beyond a yield strain of $\gamma_y \cong 0.07$. For sufficiently small strain rates, a limiting behavior is reached characterized by the gradual buildup of stress followed by sudden release via topological rearrangement. With increasing strain rates, the average stress level increases the fluctuations smooth out. These observations are consistent with the intermittent flow behavior seen in [9] as well as the claim that foams exhibit self-organized criticality in the limit of small driving rates.

The behavior of the shear stress as a function of the imposed strain rate can be quantified by an average and maximum value, shown in the main plot of Fig. 3; results are based on strains throughout the range $0 < \gamma < 10$. As evident already from the inset, the average stress increases monotonically from a constant at small $\dot{\gamma}$. The quantitative trend is well described by the Bingham-plastic model, which is often used to analyze the behavior of real foams: $\sigma_{xy} = \sigma_y + \mu_p \dot{\gamma}$, where σ_y and μ_p are phenomenological parameters called the yield stress and plastic viscosity, respectively [1]. The solid curve through the maximum stress data in Fig. 3 is a fit by this form, giving $\sigma_y = 0.020$ and $\mu_p = 4.8\tau_d$. The former is larger than $G\gamma_y$, but the same order of magnitude, and the latter is comparable to the relaxation time τ_r. A similar analysis for a 12×12 system gave $\mu_p = 10\tau_d$, again consistent with τ_r. Thus, the spherical bubble model correctly reproduces the Bingham-plastic flow behavior of foams and given insight into the value of the yield stress and plastic viscosity in terms of the linear rheological behavior.

In conclusion, a new model has been constructed for the molecular dynamics simulation of foam rheology in terms of structure and dynamics at the bubble scale, and has been shown to reproduce the hallmark behavior. The minimum set of ingredients needed to produce these phenomena include mechanism for storing and dissipating energy, as well as random packing and rearrangement effects. Such ingredients are present in other forms of condensed matter, such as emulsions, colloidal suspensions, slurries and clays, and granular materials, where inertial and/or thermal effects must also be considered. These ingredients are also present for systems such as charge density waves and disordered flux line lattices, where pinning effects are important. In this sense, the model presented here is perhaps the simplest example of a broad class of dynamical systems exhibiting elastic, plastic, and fluid behavior.

Conversations with R. Bruinsma, S. A. Langer, A. J. Liu, S. Ramaswamy, and D. A. Weitz are gratefully acknowledged. This work was partially supported by NASA.

[1] A. M. Kraynik, Annu. Rev. Fluid Mech. **20**, 325 (1988).
[2] D. M. A. Buzza, C. Y. D. Lu, and M. E. Cates, J. Phys. II **5**, 37 (1995).
[3] H. M. Princen, J. Colloid Interface Sci. **91**, 160 (1983).
[4] D. Weaire and J. P. Kermode, Philos. Mag. B **50**, 379 (1984).
[5] T. Herdtle and H. Aref, J. Fluid Mech. **241**, 233 (1992).
[6] F. Bolton and D. Weaire, Phys. Rev. Lett. **65**, 3449 (1990).
[7] S. Hutzler, D. Weaire, and F. Bolton, Philos. Mag. B **71**, 277 (1995).
[8] T. Okuzono and K. Kawasaki, J. Rheol. **37**, 571 (1993).
[9] T. Okuzono and K. Kawasaki, Phys. Rev. E **51**, 1246 (1995).
[10] D. C. Morse and T. A. Witten, Europhys. Lett. **22**, 549 (1993).
[11] T. G. Mason, J. Bibette, and D. A. Weitz, Phys. Rev. Lett. **75**, 2051 (1995).
[12] F. Bolton and D. Weaire, Philos. Mag. B **65**, 473 (1992).
[13] D. Weaire, Philos. Mag. B **51**, L19 (1985).
[14] D. J. Durian, D. A. Weitz, and D. J. Pine, Science **252**, 686 (1991).
[15] J. C. Earnshaw and M. Wilson, J. Phys. Condens. Matter **7**, L49 (1995).
[16] A. D. Gopal and D. J. Durian, Phys. Rev. Lett. **75**, 2610 (1995).